

## Reduction of Dielectric Hysteresis in Multilayered Films via Nanoconfinement

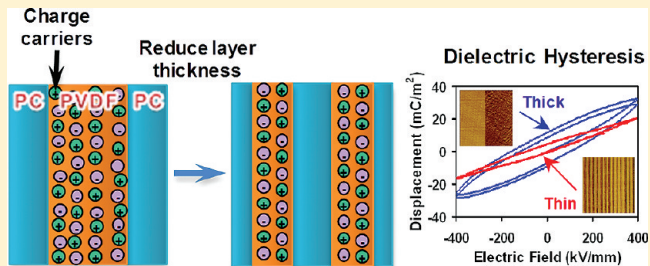
Matthew Mackey,<sup>†</sup> Donald E. Schuele,<sup>†</sup> Lei Zhu,<sup>†,\*</sup> Lionel Flandin,<sup>‡</sup> Mason A. Wolak,<sup>§</sup> James S. Shirk,<sup>§</sup> Anne Hiltner,<sup>†,||</sup> and Eric Baer<sup>†,\*</sup>

<sup>†</sup>Department of Macromolecular Science and Engineering, Case Western Reserve University, Cleveland, Ohio 44106, United States

<sup>‡</sup>LEPMI, UMR 5279, CNRS, Université de Savoie, F-73376 Le Bourget Du Lac Cedex, France

<sup>§</sup>US Naval Research Laboratory, Washington, D.C. 20375, United States

**ABSTRACT:** Micro/nanolayer coextrusion was used to fabricate polycarbonate (PC)/poly(vinylidene fluoride) (PVDF) layered films with significantly reduced dielectric losses while maintaining high energy density. The high-field polarization hysteresis was characterized for layered films as a function of PVDF layer thickness (6000 to 10 nm) and composition (10 to 70 vol % PVDF), and was found to decrease with decreasing layer thickness and PVDF content. To gain a mechanistic understanding of the layer thickness (or nanoconfinement) effect, wide-angle X-ray diffraction, polarized Fourier transform infrared spectroscopy, and broadband dielectric spectroscopy were employed. The results revealed that charge migration, instead of dipole flipping, was responsible for the hysteresis in multilayered films. The absence of PVDF dipole-flipping was attributed to the nonuniform electric field distribution in the layered structure, where the field in PVDF layers were calculated to be significantly lower than that in PC layers due to large contrast in dielectric constant ( $\sim 3$  for PC versus  $\sim 12$  for PVDF). The charges were likely to be impurity ions in the form of catalyst residue or surfactants from suspension polymerization. The characteristics of the dielectric spectroscopy relaxation indicated that ions mostly existed in the PVDF layers, and PC/PVDF interfaces prevented them from entering adjacent layers. Therefore, as the layer thickness decreases to nanometer scales, the amount of ion movement, dielectric loss, and hysteresis were decreased. This study provides clear evidence of the nanoconfinement effect in multilayered films, which advantageously decreases the hysteresis loss.



### INTRODUCTION

Capacitors are vital in nearly all microelectronics and electronic devices, ranging from cell phones and computers to automotive vehicles and power systems.<sup>1–3</sup> The common uses include signal coupling/decoupling and filtering, high current sourcing, power conditioning, and pulsed power (or energy storage). Currently, there are several important motivations for developing dielectric capacitors with increased energy density and low loss. First, it is necessary for capacitors to keep pace with the global trend of electronics miniaturization. Second, with the drive to decrease fossil fuel dependence, compact/lightweight and reliable capacitors are required for applications such as hybrid electric vehicles<sup>4</sup> and grid converters for renewable energy sources.<sup>5</sup> The maximum energy density that can be stored in an insulating material is proportional to the dielectric constant times the square of the breakdown strength.<sup>6</sup> Therefore, highly insulating materials with both a high dielectric constant and high breakdown strength are desired. To maintain high performance and reliability, it is also necessary to maintain low losses (i.e., low-field dissipation factor and high-field hysteresis loss) since losses reduce the discharged energy density, cause dielectric heating, and limit the frequency response of the capacitor.<sup>1</sup>

Polymer dielectrics have recently attracted substantial research interest because of their excellent manufacturing/processing advantages and electrical insulating properties. From a manufacturing point of view, polymers are easy to produce and process on a large scale, which makes them inexpensive. They are also lightweight with good mechanical properties. Regarding their electrical properties, polymers generally have a high breakdown strength and low losses.<sup>7</sup> Two widely used state-of-the-art polymer dielectrics are biaxially oriented polypropylene (BOPP) and poly(ethylene terephthalate) (PET), which have the following measured properties: material level energy density of 5–6 J/cm<sup>3</sup> at breakdown, dielectric constant of 2–3, breakdown strength of 600–700 MV/m, and tan  $\delta$  of 0.0003–0.002.<sup>2</sup>

In spite of extensive and far-reaching research efforts, realization of high performance dielectric materials with increased energy density and low loss is still an important goal. One method of improving the energy density and performance is to combine two or more different materials by blending or *in situ* polymerization. Several common fillers for

Received: October 12, 2011

Revised: January 9, 2012

Published: February 3, 2012

**Table 1.** Details of the 50PC/50PVDF Multilayered Films and the Corresponding Thermal Properties

composition (vol %) (PC/PVDF)	no. of layers	film thickness ( $\mu\text{m}$ )	PVDF layer thickness (nm)	PVDF crystallinity (%)	$T_m$ ( $^{\circ}\text{C}$ )	$T_c$ ( $^{\circ}\text{C}$ )
PVDF control	-	12	-	51	171	131
PC control	-	12	-	-	$T_g$ : 150	-
50/50	2	12	6000	48	171	132
50/50	2	6	3000	50	171	131
50/50	8	12	1500	46	171	131
50/50	8	6	750	45	171	132
50/50	32	12	380	45	171	130
50/50	32	6	187	43	172	132
50/50	256	12	50	42	171	128
50/50	256	6	25	42	171	129

high energy density polymer nanodielectrics include barium titanate,<sup>8–12</sup> lead zirconate titanate,<sup>13</sup> and titanium dioxide.<sup>14,15</sup> Other techniques aim to modify BOPP (or PET)<sup>16</sup> or synthesize specialized copolymers and terpolymers, e.g., poly(vinylidene fluoride-*co*-chlorotrifluoroethylene) [P(VDF-CTFE)] and P(VDF-*co*-trifluoroethylene-*co*-chlorotrifluoroethylene) [P(VDF-TrFE-CTFE)].<sup>6,17,18</sup> Often, the approaches produce an enhancement in one of the properties (e.g., energy density) but a reduction in another (e.g., dielectric and hysteresis losses). Other common issues include commercial viability, scale-up, cost, and mechanical/thermal stability, which are difficult for newly synthesized materials.<sup>19,20</sup>

To improve electrical properties while maintaining mechanical integrity and commercial viability requirements, we have used the novel polymer processing technique of micro/nanolayer coextrusion to produce layered structures. This processing technique includes the combination of 2 or 3 polymers in an ABABABAB, ABCABCABC, or ABCBABC configuration, creating films with 2 to 4096 layers and layer thicknesses ranging from tens of micrometers down to less than 10 nm.<sup>21</sup> Prior research has shown that useful changes occur in the mechanical, optical,<sup>22–24</sup> and transport properties,<sup>25</sup> as the layer thickness is reduced to nanometer scales. From a dielectric standpoint, analogous changes are expected and electrical properties can be optimized by independently varying the layer thickness and film composition. The layered film containing one high dielectric constant material [P(VDF-*co*-hexafluoropropylene), P(VDF-HFP)] and one high breakdown strength material [polycarbonate (PC)] has been previously studied and shown to provide significant enhancements in breakdown strength.<sup>26,27</sup>

In this report, the nanoconfinement effect from multilayering of PC and PVDF on reducing low-field dielectric and high-field hysteresis losses is explored. It is found that ion migration in PVDF layers, rather than PVDF dipole switching, is responsible for both dielectric and hysteresis losses. Note that the PVDF is synthesized by suspension polymerization. Therefore, the ionic impurity should originate from surfactant residue. On the basis of a simulation study using the diffusion model by Sawada,<sup>28,29</sup> the diffusion coefficient and concentration of the impurity ions were estimated to be  $2 \times 10^{-13} \text{ m}^2/\text{s}$  and <1 ppm (by weight), respectively. By decreasing the PVDF layer thickness down to a few tens of nanometers, both low and high field losses can be significantly reduced. On the basis of this finding, the synergistic effect of thin layers and additives on the physical properties may open a door to new engineering practice in many other applications.

## EXPERIMENTAL SECTION

**Materials.** Two polymers were used in this study, one for its high breakdown strength and the other for its high dielectric constant. PC, Calibre 200–6 with a molecular weight of 24 500 g/mol from Dow Chemical Company, was chosen as the high breakdown strength material. PVDF homopolymer, Solef 6010 with a molecular weight of 64 000 g/mol from Solvay Solexis, was chosen as the high dielectric constant material. A set of PC/PVDF multilayered films was produced using microlayer coextrusion (Table 1). The films were coextruded with sacrificial polyethylene (PE) skin layers on both sides of the layered film in order to improve the film surface smoothness, handleability, and immunity to damage. This skin was peeled off before any measurements were carried out. In addition to the 50/50 PC/PVDF films in Table 1, compositions of 90/10, 70/30, 30/70, and 10/90 were also produced. A coextrusion temperature of 250 °C was chosen based on the rheological compatibility of the two polymers. The polymer rheology was characterized using a melt flow indexer (MFI), on Kayeness Galaxy 1, at a shear rate that is similar to extrusion conditions (10 s<sup>-1</sup>). Prior to processing the PC resin, it was dried in a vacuum oven at 80 °C for 48 h.

**Atomic Force Microscopy (AFM).** The layered film cross sections were imaged using AFM. The samples were prepared by embedding the films in epoxy and microtoming at –40 °C with an ultramicrotome (Leica EM FC6). Phase and height images of the cross sections were recorded simultaneously at ambient temperature in air using the tapping mode of a Nanoscope IIIa MultiMode scanning probe (Digital Instruments, Santa Barbara, CA).

**Dielectric Hysteresis Measurements.** Electric displacement–electric field ( $D$ – $E$ ) hysteresis measurements were carried out on a Premiere II ferroelectric tester from Radiant Technologies, Inc. The applied voltage was a bipolar triangular waveform at 1 Hz. An electrostatic sandwich technique was used to apply electrodes, which were 5.8  $\mu\text{m}$  metallized BOPP films, on both sides of the film.<sup>30</sup> An 80  $\mu\text{m}$  thick Kapton mask with a 1 cm diameter hole was used to control the area under high fields. In each sample, electric fields from 100 to 500 MV/m were applied to the sample in 50 MV/m increments. This electrostatic sandwich setup performed better without any insulating oils because the oil could prevent two metallized BOPP films from coming together and establishing a tight contact with the test film. To ensure safety, all high field measurements were remotely controlled with a computer.

**X-ray Diffraction.** Wide-angle X-ray diffraction (WAXD) patterns were obtained by aligning the incident X-ray beam parallel to the extrusion direction (ED) of the film. The measurements were performed on a Rigaku MicroMax-002<sup>+</sup> diffractometer at 45 kV and 0.88 mA. A Confocal Max-Flux optics was used with a sealed tube microfocus X-ray source, giving a highly focused beam of monochromatic Cu  $K\alpha$  radiation ( $\lambda = 0.154 \text{ nm}$ ). The sample-to-detector distance was 140 mm, and the diffraction angle was calibrated using a CaF<sub>2</sub> standard. The patterns were collected using an image plate with a 50  $\mu\text{m}$  pixel size.

**Electric Field Dependent Polarized Fourier Transform Infrared (FTIR).** Polarized FTIR under electric field was carried out on a Nexus 870 FTIR ESP from Nicolet with the polarizer fixed at the

perpendicular configuration, i.e., the angle between the film stretching direction and the polarizing light was  $90^\circ$ . Films were stretched about four times at  $120\text{ }^\circ\text{C}$  using a homemade uniaxial stretching machine in a Blue-M gravity oven. Carbon electrodes were evaporated onto both sides of the film using a Denton Bench Top Turbo III high vacuum evaporator. The thickness of carbon electrodes was optimized so that the resulting resistance was several  $\text{k}\Omega$  with a baseline transmittance of 80–90%.<sup>31–33</sup> High electric fields were supplied with a Matsusada AMT-20B10-B high voltage amplifier.

**Dielectric Spectroscopy.** Broadband dielectric spectroscopy measurements were performed on a Novocontrol unit (0.001 Hz to 100 kHz, 25 to  $200\text{ }^\circ\text{C}$ ) under a vacuum of 40 mTorr. Sample was prepared by evaporating 30 nm thick aluminum electrodes with 1 cm diameter to both sides of the test film.

## RESULTS AND DISCUSSION

**Effect of Layering on High-Field Polarization Hysteresis.** The layer integrity and uniformity were examined using phase contrast atomic force microscopy (AFM), as shown in Figure 1. There were no structural defects in the multilayered

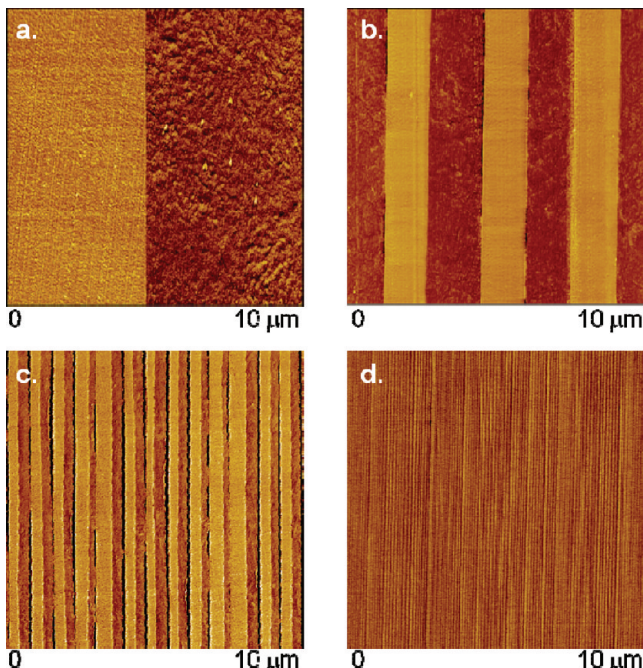


**Figure 1.** AFM phase images of 50PC/50PVDF layered film cross sections. Key: (a) 2 layers (12  $\mu\text{m}$ /6000 nm); (b) 8 layers (12  $\mu\text{m}$ /1500 nm); (c) 32 layers (12  $\mu\text{m}$ /375 nm); (d) 256 layers (12  $\mu\text{m}$ /50 nm). The light and dark colored layers are PC and PVDF, respectively.

films such as layer breakup or interlayer connection, which is the advantage of forced assembly using microlayer coextrusion.<sup>21,25</sup> The layer thickness and standard deviation were determined from the AFM images in Figure 1 to be  $6200 \pm 780$  nm,  $1600 \pm 160$  nm,  $400 \pm 90$  nm, and  $50 \pm 10$  nm for 50PC/50PVDF 2-, 8-, 32-, and 256-layer films, respectively. These measured thicknesses are in good agreement with the nominal layer thicknesses given in Table 1 in the Experimental Section. Here, an individual film is named as  $xx\text{PC}/yy\text{PVDF}$  ( $LL\text{ }\mu\text{m}/ZZ\text{ nm}$ ), where  $xx$  and  $yy$  are volume percentages of PC and PVDF,  $LL$  is the total film thickness, and  $ZZ$  is the PVDF layer thickness. This nomenclature will be used throughout the paper.

To determine the effect of layer confinement on  $D-E$  hysteresis, measurements were carried out on PC/PVDF

layered films and controls. For clarity, a single field sweep at 400 MV/m is shown for the two controls. For the layered films, field sweeps at 100, 200, 300, and 400 MV/m are shown. The PC control exhibited low hysteresis, which was expected for linear dielectric materials, and the PVDF control had a large hysteresis loop with dipole saturation at high fields, which was typical of ferroelectric materials (Figure 2a).<sup>34</sup> The hysteresis

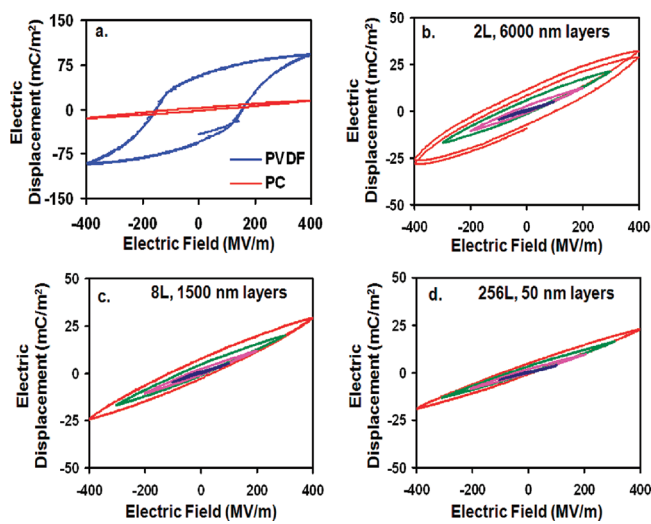


**Figure 2.**  $D-E$  hysteresis loops of monolithic controls and 50PC/50PVDF layered films with different layer thicknesses. Key: (a) monolithic PC and PVDF controls, 12  $\mu\text{m}$  thick; (b) 2 layers (12  $\mu\text{m}$ /6000 nm); (c) 8 layers (12  $\mu\text{m}$ /1500 nm); (d) 256 layers (12  $\mu\text{m}$ /50 nm). Each loop at a given electric field has two poling cycles. For parts b-d, blue, magenta, green, and red loops correspond to the poling field being 100, 200, 300, and 400 MV/m, respectively.

behavior of layered films showed intermediate levels of electric displacement relative to the controls, i.e., larger loops than PC but no dipole saturation at high fields (400–500 MV/m) as seen for the PVDF control (Figure 2).

The effects of layer thickness, electric field, and film composition on dielectric hysteresis were studied for the PC/PVDF layered films. In parts b-d of Figure 2, reducing layer thickness caused a substantial decrease in the hysteresis. These results were quantified and generalized by calculating the hysteresis loop area as a function of layer thickness for several different compositions and electric fields (Figure 3). It was found that thinner layers had a beneficial effect on the hysteresis at different electric fields (300–500 MV/m) and compositions (10–70 vol % PVDF) (see Figure 3). When independently studying the effects of composition and electric field on hysteresis, the hysteresis loop area increased with increasing the PVDF content and electric field. When the PVDF volume fraction was 90 vol %, the high-field hysteresis loop substantially opened up and became similar to that of PVDF in Figure 2A (data not shown), suggesting that when the PC layer thickness was too thin as compared to the thickness of PVDF, the PC layers had almost no effect on reducing the hysteresis loss. Therefore, no comparison was made for PC/PVDF 10/90 multilayered films in Figure 3.

The above results provided us the following information. First, the composition effect indicated that PVDF layers were responsible for the hysteresis, which was consistent with the large hysteresis of the PVDF control. Regarding the effect of electric field, a higher field caused a greater electric displace-

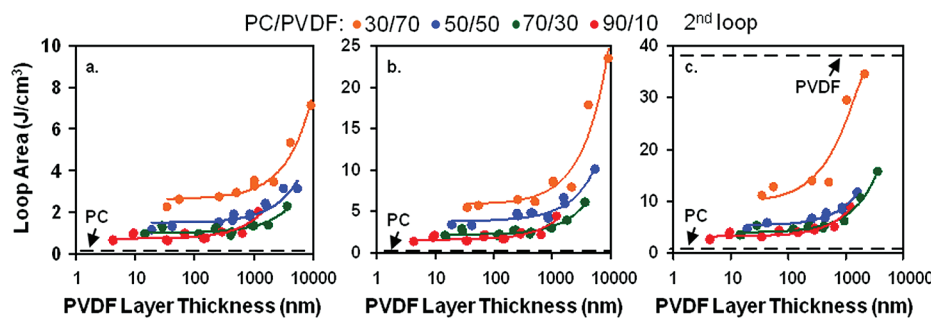


**Figure 3.** Hysteresis loop area of layered films as a function of PVDF layer thickness for different layer compositions at (a) 300 MV/m, (b) 400 MV/m, and (c) 500 MV/m, respectively.

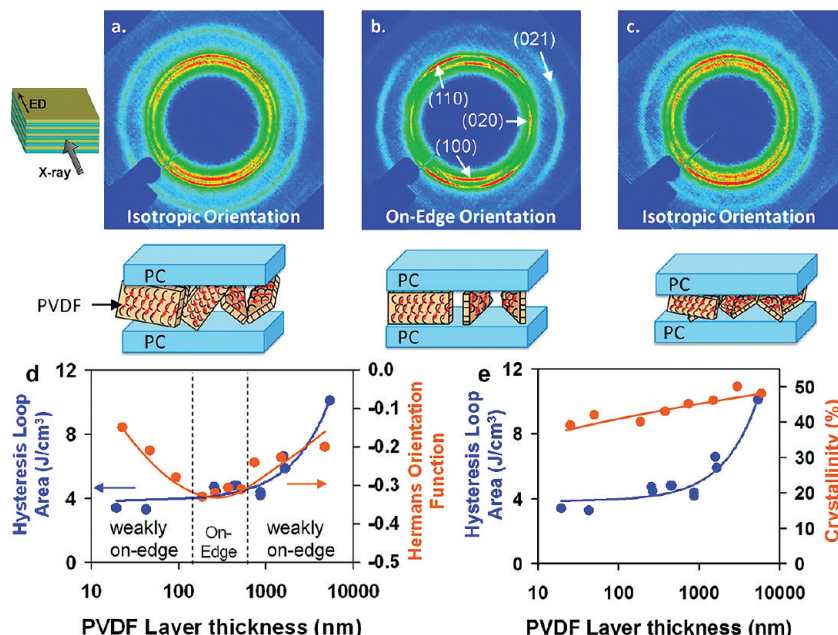


**Figure 4.** WAXD patterns of 50PC/50PVDF layered films: (a) 8 layers (12  $\mu\text{m}$ /1500 nm); (b) 32 layers (12  $\mu\text{m}$ /380 nm); (c) 256 layers (12  $\mu\text{m}$ /50 nm). The X-ray beam is parallel to the extrusion direction (ED, see the inset scheme). (d) Hysteresis loop area and Hermans orientation function as a function of layer thickness for 50PC/50PVDF layered films. (e) Hysteresis loop area and PVDF crystallinity as a function of layer thickness for 50PC/50PVDF layered films.

ment, part of which originated from the irreversible polarizations (e.g., dipoles in ferroelectric crystals and ions in the amorphous phase).<sup>7</sup> The mechanism behind the layer thickness effect was, however, not immediately apparent. To determine why nanolayers had reduced hysteresis, polarized FTIR and broadband dielectric spectroscopy experiments were carried out to differentiate the effect of dipole switching from that of ion migration.

#### Ferroelectric Dipole Switching in Multilayered Films.

The large dielectric hysteresis in PVDF-based polymers is most commonly attributed to dipolar switching where the dipoles in ferroelectric crystals rotate in response to an applied field.<sup>34</sup> In contrast to ferroelectric PVDF, paraelectric materials like PC, PET, and BOPP exhibit almost no hysteresis because orientational polarization does not exist in the sample.<sup>7</sup> Knowing that the hysteresis in layered films can originate from orientational polarization in PVDF layers, we propose that the possible hysteresis mechanism in layered films might originate from dipole switching, which can be experimentally determined using field-dependent polarized FTIR on uniaxially oriented films.

Because dipole switching is typically associated with ferroelectric crystals, we first examined the crystal orientation in the PVDF layers as a function of layer thickness, using WAXD. With decreasing the layer thickness, the crystal orientation went from weakly on-edge (Figure 4a) to on-edge (Figure 4b) and back to weakly on-edge (Figure 4c) with a maximum on-edge orientation occurring in films with 200 nm PVDF layers (Figure 4d). Here, weakly on-edge indicated that the crystallographic *a*-axes had some tendency of being perpendicular to the layers. This unexpected trend was reproducible and some explanation of the behavior was given in ref 35. The on-edge orientation is expected to contribute to increased rather than decreased hysteresis,<sup>36</sup> because the  $\text{CH}_2\text{CF}_2$  dipoles are nearly perpendicular to the chain axes and in a plane parallel to applied field. Therefore, the WAXD results in Figure 4d implied that dipole switching should not correlate with the reduced hysteresis as PVDF layer thickness decreased. The crystallite size can be estimated using the Scherrer equation from the peak width of WAXD reflections in Figure 4. The peak width and thus crystallite size of WAXD reflections was not much affected by the layer thickness. Therefore, the reduced hysteresis could not be attributed to

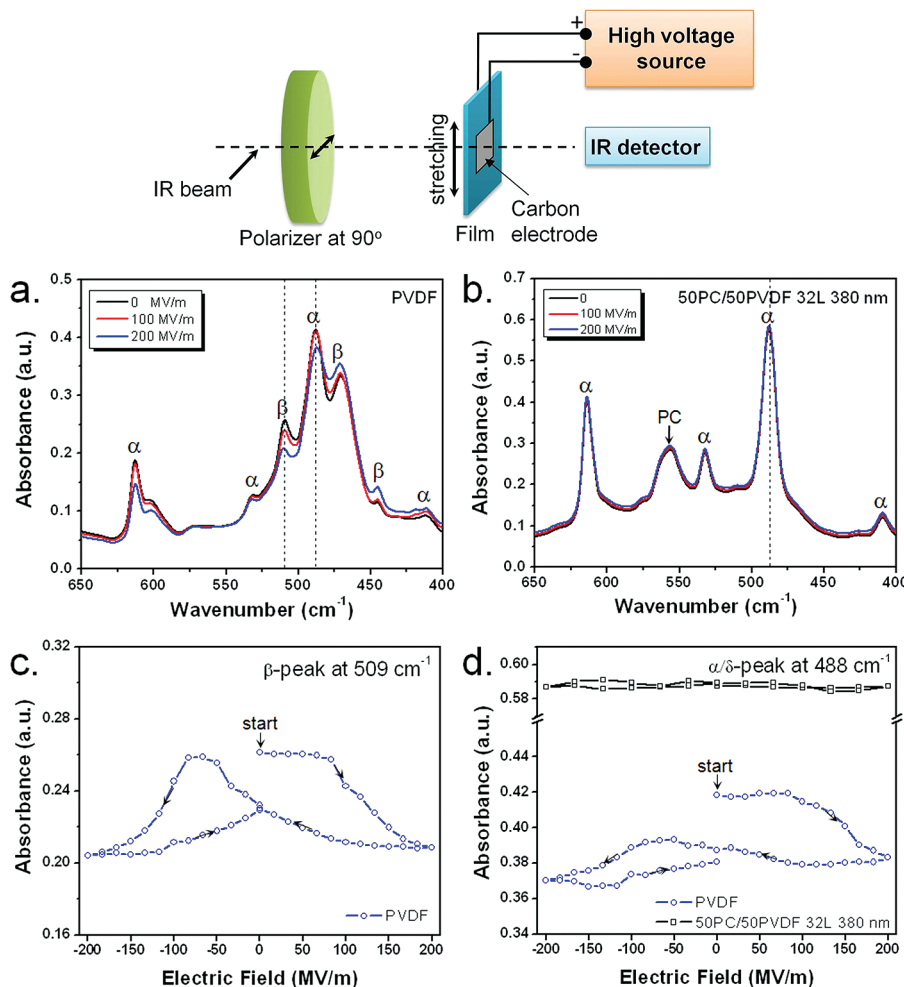


**Figure 5.** Polarized FTIR spectra of uniaxially oriented (a) PVDF and (b) 50PC/50PVDF (12  $\mu\text{m}$ /380 nm) films under different electric fields. The stretching ratios were 400% and 370% for PVDF and 50PC/50PVDF (12  $\mu\text{m}$ /380 nm) films, respectively. The polarized light is perpendicular to the film stretching direction (see the top panel for the polarized FTIR experimental setup). For clarity, each spectrum in part b is offset by 0.005 (absorbance) to avoid complete overlap. (c) The  $\beta$ -peak absorbance at  $509 \text{ cm}^{-1}$  and (d) the  $\alpha/\delta$ -peak absorbance at  $488 \text{ cm}^{-1}$  as a function of electrical field for uniaxially oriented PVDF and 50PC/50PVDF (12  $\mu\text{m}$ /380 nm) films. The start and change of electric field are shown by arrows in (c) and (d).

changes in the crystallite size.<sup>37</sup> Because the dipole switching-derived hysteresis can only occur in the crystals, the crystallinity of PVDF as a function of layer thickness was also investigated (Figure 4e). The crystallinity decreased from 51% to 42% as the PVDF layer thickness decreased from 6000 to 25 nm. A 9% decrease in crystallinity, however, could not simply account for such a substantial decrease in hysteresis (Figure 4e).

Field-dependent polarized FTIR spectra for uniaxially oriented PVDF and 50PC/50PVDF (12  $\mu\text{m}$ /380 nm) films are shown in Figure 5, parts a and b, respectively. Uniaxial stretching was used to maximize the  $509 \text{ cm}^{-1}$  absorbance intensities by orienting the  $\text{CF}_2$  dipoles parallel to the polarized light. Our experimental result showed that uniaxial stretching did not change the shape and magnitude of hysteresis loops as compared to the unstretched film. The polarized light was perpendicular to the film stretching direction (see the top panel of Figure 5). Because the PVDF control film was stretched at  $120^\circ\text{C}$ , both  $\alpha$  and  $\beta$  characteristic peaks were seen in Figure 5a.<sup>34,38</sup> Upon varying the applied field, the absorbance for both  $\beta$  and  $\alpha/\delta$  peaks changed (note that PVDF  $\alpha$ -phase will transform into  $\delta$ -phase upon electric poling above  $100 \text{ MV/m}$ ).<sup>39</sup> Typical results for

the  $\beta$ -peak at  $509 \text{ cm}^{-1}$  and  $\alpha/\delta$ -peak at  $488 \text{ cm}^{-1}$  are shown in Figure 5, parts c and d, respectively. As expected, butterfly shaped hysteresis loops were observed in both figures, indicating that dipoles switched in response to the applied field.<sup>34</sup> For the 50PC/50PVDF (12  $\mu\text{m}$ /380 nm) film, only  $\alpha$ -phase was observed despite that it was stretched at  $120^\circ\text{C}$  to 3.7 times its original length (see Figure 5b). Note that there was no significant interference of the PC absorbance in the range between  $400$  and  $650 \text{ cm}^{-1}$ . In addition, the absorbance of the  $\alpha/\delta$ -peak at  $488 \text{ cm}^{-1}$  does not vary with the applied electric field. From this result, we conclude that there is no dipole switching in PC/PVDF layered films. This can be understood from the following analysis. Assuming that relative dielectric constants for PC and PVDF are  $\epsilon_{r,\text{PC}} = 3^{26}$  and  $\epsilon_{r,\text{PVDF}} = 12$ ,<sup>27,36</sup> respectively, the nominal electric fields ( $E$ ) in PC and PVDF layers in a serial capacitor model are as follows:<sup>27,40</sup>

$$E_{\text{PC}} = E_0 \left[ \Phi_{\text{PC}} \left( 1 - \frac{\epsilon_{r,\text{PC}}}{\epsilon_{r,\text{PVDF}}} \right) + \frac{\epsilon_{r,\text{PC}}}{\epsilon_{r,\text{PVDF}}} \right]^{-1} \quad (1)$$

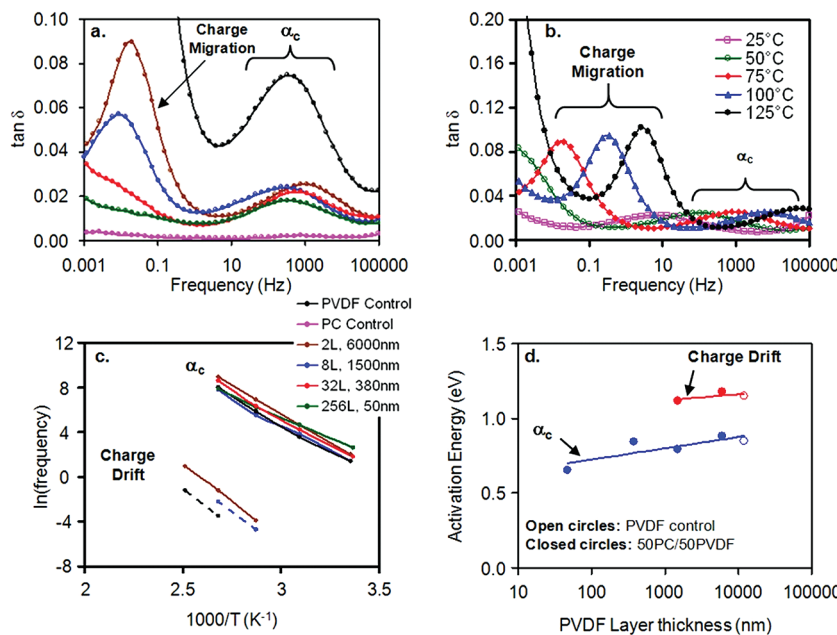


**Figure 6.** Dielectric spectroscopy of (a) 50PC/50PVDF layered films at 75 °C for different layer thicknesses and (b) the 50PC/50PVDF (6 μm/3000 nm) film as a function of frequency at different temperatures. Activation energy plots of 50PC/50PVDF (12 μm) layered films: (c)  $\ln(\text{peak frequency})$  as a function of reciprocal temperature and (d) activation energy as a function of layer thickness for both charge migration and  $\alpha_c$  relaxation processes. The legends in part c are also for part a.

$$E_{\text{PVDF}} = E_0 \left[ \phi_{\text{PC}} \left( \frac{\epsilon_r, \text{PVDF}}{\epsilon_r, \text{PC}} - 1 \right) + 1 \right]^{-1} \quad (2)$$

Here  $E_0$  is the external electric field and  $\phi_{\text{PC}}$  is the volume fraction of PC. When the external electric field is 200 MV/m for a 50PC/50PVDF film, the nominal fields in PC and PVDF layers are calculated to be 320 and 80 MV/m, respectively. In addition, the coercive field could increase as the PVDF thickness decreased to the nanometer range, making dipole switching more difficult in layered films.<sup>41,42</sup> Therefore, we consider that it is the low nominal electric field in thin PVDF layers (80 MV/m) that prevent the dipole switching in the layered films. Further increase the poling electric field may be able to induce dipole flipping in PVDF. Nevertheless, this may exceed the electric breakdown field of the film and cannot be experimentally achieved.

Given no dipole-flipping in PVDF, we would like to ask: What is the possible reason for the reduced hysteresis as the PVDF layer thickness decreases? As we know, there are five types of polarization in polymers, namely, electronic, atomic, (dipolar) orientational, ionic, and interfacial polarizations.<sup>7</sup> Electronic and atomic polarizations take place in the optical and infrared frequencies. Therefore, there should be no loss at all from electronic and atomic polarizations at the 10 Hz poling frequency. Because PVDF dipoles do not flip, the observed hysteresis can only originate from ionic and/or interfacial (or Maxwell–Wagner–Sillars<sup>7</sup>) polarizations. If the observed hysteresis originates from interfacial polarization, the more layers in the multilayer film will have more interfaces and in turn will result in greater hysteresis loss. This is contradictory to the above experimental observation. Therefore, the observed hysteresis can only originate from ionic polarization. The question then is: Why the hysteresis decreases as the PVDF layer thickness decreases in PC/PVDF multilayer films?

**Charge Migration.** If charge migration exists, broadband dielectric spectroscopy can be used to detect the ion motion.<sup>43,44</sup> Measurements were carried out on the controls and 50PC/50PVDF layered films as a function of layer thickness and temperature (Figure 6). Two dielectric relaxations were observed over the frequency (0.001–100 kHz) and temperature (25–125 °C) ranges tested: one at a high frequency (1 kHz at 75 °C) which is not affected by layer thickness and another at a low frequency (0.02 Hz at 75 °C) which is layer thickness dependent. The high frequency relaxation peak occurred in both the PVDF control and layered films and is known in the literature as the  $\alpha_c$  relaxation of  $\alpha$ -form PVDF associated with the dipole wagging along the helical axes.<sup>36,45</sup> The  $\alpha_c$  relaxation was not significantly affected by layer thickness because the molecular origins are much smaller than the thinnest layers. In contrast, the low frequency relaxation was affected by layer thickness, which indicates that the underlying mechanism had a length scale on the order of micrometers to nanometers; these characteristics are typical of ion migration.<sup>43,44,46</sup> On the basis of the  $\tan \delta$  of the controls (Figure 6a), the impurity ions are predominantly in the PVDF layers rather than the PC layers because the  $\tan \delta$  of the PVDF control increased sharply at low frequencies due to ionic conduction while the PC control was relatively flat over the entire frequency range (Figure 6a). The dielectric spectra for the 50PC/50PVDF (6 μm/3000 nm) film were also collected at temperatures ranging from 25 to 125 °C (Figure 6b). As expected from time–temperature superposition, the relaxations shifted to higher frequency with increasing temperature. This was used to calculate the activation energies of both charge migration and  $\alpha_c$  processes for the layered films and PVDF control as a function of the layer thickness (Figure 6, parts c and d). Linear relationships between  $\ln(\text{peak frequency})$  and reciprocal temperature were obtained for both processes (Figure 6c), indicating that Arrhenius equation could be used to obtain the activation energies. Values of 0.85 and 1.15 eV (1

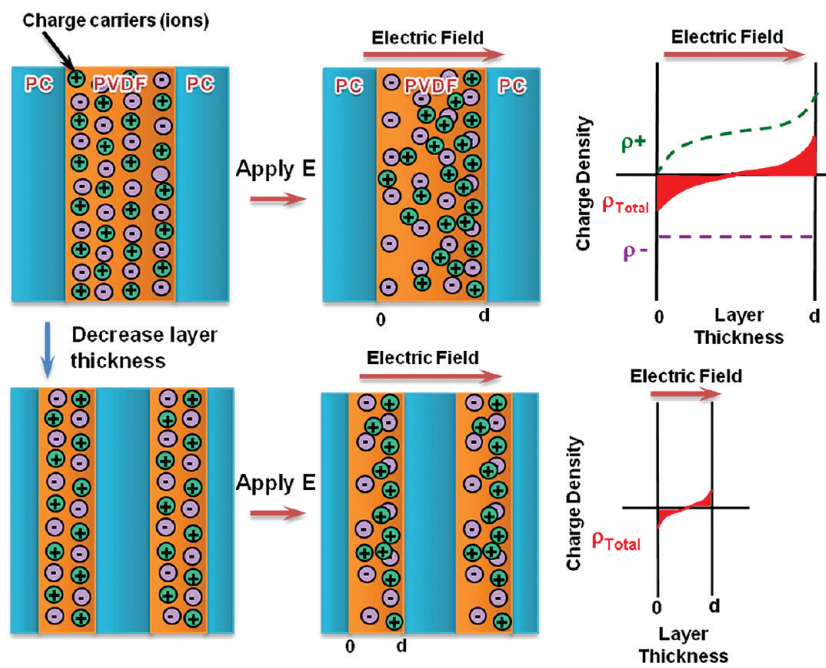


**Figure 7.** Schematic of charge migration in layered films: (top panel) thick layers and (bottom panel) thin layers. Both positive and negative ions are needed to maintain a zero net charge. For simplicity, it is assumed that only one of the charge carriers moves. After an electric field is applied, there is a gradient in charge concentration. Compared with thick PVDF layers, thin PVDF layers have less charge motion and total charge buildup.

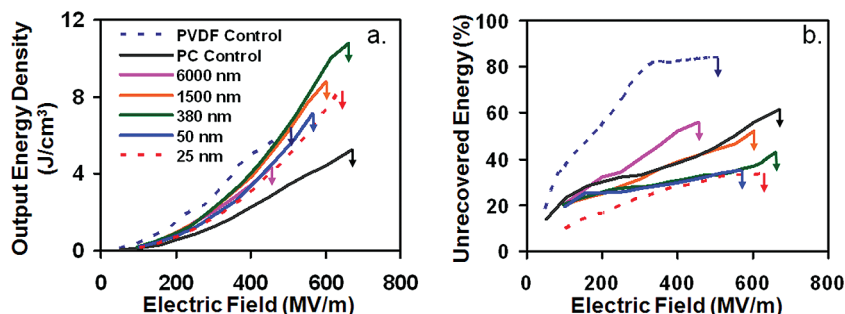


**Figure 8.** (a) Output energy density and (b) percent unrecovered energy of 50PC/50PVDF films as a function of electric field. To confirm reliability, each measurement was repeated twice.

eV = 96.3 kJ/mol) were obtained for the activation energies in the  $\alpha_c$  and charge migration relaxations, respectively (Figure 6d). The activation energies of the  $\alpha_c$  and charge migration processes were comparable with those reported in the literature.<sup>44,47,48</sup> Regarding the effect of layer thickness, the  $\alpha_c$  activation energy decreased as the layers became thinner. This might be caused by the greater fraction of interphase material in films with thinner layers. The interphase usually exhibits a set of properties different from the bulk material.<sup>49,50</sup>

The details of charge migration<sup>51</sup> adapted to a layered film structure are explained as follows. Ions, in the form of surfactant residue (Solef 6010 is synthesized from suspension polymerization according to the manufacturer datasheet),<sup>7</sup> are initially homogeneously dispersed in the PVDF layer. To maintain charge neutrality, the same number of positive and negative charges exists. The charges are also assumed to be confined to their respective layers because the interfaces act as barriers to ion motion as a result of the potential barrier.<sup>7</sup> Alternatively, due to the high resistivity of PC (i.e., value of  $10^{17}$   $\Omega\text{-cm}$  from manufacturer datasheet) compared to PVDF (i.e.,  $10^{14}$   $\Omega\text{-cm}$  from manufacturer datasheet), it is possible that the PC layers and interfaces act as blocking electrodes causing the

ions to be confined in the PVDF. When an electric field is applied, one or both of the positive and negative charges migrate to the layer interface producing a drift current and an ion concentration gradient. The migration may occur through the free volume in a manner analogous to gas diffusion in polymers.<sup>52</sup> The charges build up at the layer interface(s) until the drift current is balanced by the diffusion current (due to thermal motion and the repulsion of like charges) (top panel in Figure 7). In films with thinner PVDF layers, the amount of ion motion and charge buildup at the interface is lower (bottom panel in Figure 7), which decreases the hysteresis at high fields and the amplitude of the charge migration dielectric loss peak at low fields. In addition, the small charge separation in thin layers allows them to relax to equilibrium faster than in thick layers, which allows for improved output energy density. Because the concentration of ionic impurity is estimated to be less than 1 ppm (by weight),<sup>28</sup> it is difficult to identify the chemical structure of these impurity ions.

**Effect of Layering on Output Energy Density and Hysteresis Loss.** Dielectric hysteresis directly affected the output (or discharged) energy density and percent unrecovered energy, which were determined by integrating the D-E

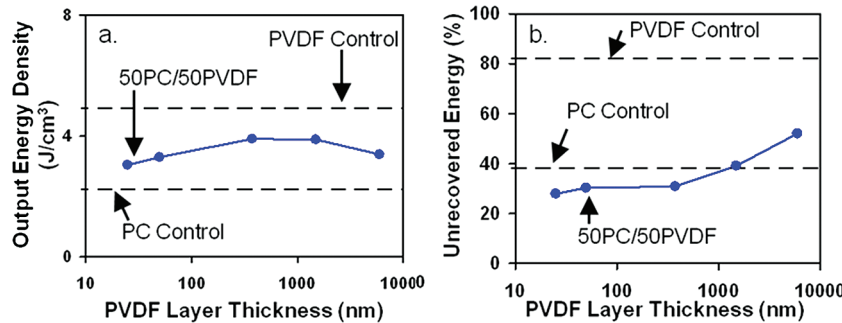


**Figure 9.** (a) Output energy density and (b) percent unrecovered energy of 50PC/50PVDF films as a function of layer thickness at 400 MV/m.

hysteresis loop of 50PC/50PVDF layered films and controls (Figure 8). Details of this calculation can be found in ref 19. The PVDF control had the highest output energy density at a given electric field below 450 MV/m, whereas the PC control had the lowest. The 50PC/50PVDF layered films were between these two controls; however, the enhanced breakdown strengths of the layered films resulted in higher output energy densities (e.g., the output energy density for the 50PC/50PVDF (12  $\mu m$ , 380 nm) was as high as 11  $J/cm^3$ ). Regarding the percent unrecovered energy, both layered films and PC control had significantly lower unrecovered energy than the PVDF control. The percent unrecovered energy also decreased as the layers became thinner. For example, for the 50PC/50PVDF (12  $\mu m$ , 380 nm) film the percent unrecovered energy density was lower than that of the PC control while still having an increased output energy density at breakdown. This indicated that the confined PVDF/PC layers were more efficient at discharging electric energy compared to the PC bulk control because the ion migration was hindered by the layered structure and interfaces. The result also showed that the 2-layer film had a low breakdown strength, indicating that more than two layers were required for high breakdown strength. A cross-plot of Figure 8 was produced at 400 MV/m to illustrate the layer thickness effect (Figure 9). Obviously, the layered structure with the PVDF layer thinner than 380 nm was effective at reducing hysteresis while also enhancing the output energy density.

## CONCLUSIONS

Multilayered films with alternating PC and PVDF were fabricated with layer thicknesses ranging from 6000 nm to less than 10 nm and compositions from 10 to 70 vol % PVDF. The layered structure provided a beneficial effect, i.e., the hysteresis decreased with decreasing layer thickness. Using polarized FTIR and broadband dielectric spectroscopy techniques to investigate dipole switching and charge migration, respectively, the underlying mechanism responsible for the high-field hysteresis was determined to be charge migration in the PVDF layers. More specifically, the dielectric spectra of the layered films exhibited a low frequency relaxation process ( $E_a = 1.15$  eV), which was attributed to charge migration and could be attenuated by decreasing layer thickness. This indicated that the layered structure and interfaces (or PC blocking layers) prevented the charge species from passing from one layer to the next. In films with thinner PVDF layers, the amount of ion motion and charge buildup at the interface was minimized. This in turn decreased the amplitude of the charge migration-induced dielectric loss peak and hysteresis. Therefore, layered structures can be utilized to

eliminate the low and high field losses in impure materials, which is very beneficial since chemical purification processes are time-consuming and costly. The effect of improved hysteresis in the layered films was significant because they could achieve increased energy density and reduced loss at the same time. For example, the 50PC/50PVDF (12  $\mu m$ /380 nm) film had an output energy density of 11  $J/cm^3$  but a percent unrecovered energy significantly lower even than that of the PC control. These findings also have important practical implications in other electronic applications that employ polymeric materials (i.e. semiconductor materials, liquid crystal displays, and electrical insulation). For insulating materials, it is desirable to remove and prevent the generation of charge carriers that may cause ionic or dc conduction. Other applications, however, may benefit from added ions to exploit ionic conduction. The multilayering technique demonstrated here has the potential for producing structures with enhanced properties for many of these other applications.

## AUTHOR INFORMATION

### Corresponding Author

\*E-mail: lxz121@case.edu (L.Z.); exb6@case.edu (E.B.).

### Notes

<sup>†</sup>Professor Anne Hiltner passed away in September 2010.

## ACKNOWLEDGMENTS

This research was generously supported by the National Science Foundation through the Center for Layered Polymeric Systems (CLIPS) Science and Technology Center (DMR-0423914) and the Office of Naval Research (N00014-10-1-0349). Jung-Kai Tseng is acknowledged for carrying out the polarized FTIR experiments.

## REFERENCES

- (1) Sarjeant, W. J.; Zirnheld, J.; MacDougall, F. W. *IEEE Trans. Plasm. Sci.* **1998**, 26, 1368–1392.
- (2) Sarjeant, W. J.; Clelland, I. W.; Price, R. A. P. *IEEE*. **2001**, 89, 846–855.
- (3) Tan, Q.; Irwin, P.; Cao, Y. *IEEE Trans. Fund. Mater.* **2006**, 126, 1152–1159.
- (4) Husain, I., *Electric and Hybrid Vehicles: Design Fundamentals*; CRC Press: Boca Raton, FL, 2010.
- (5) Teodorescu, R.; Liserre, M.; Rodríguez, P., *Grid Converters for Photovoltaic and Wind Power Systems*; Wiley: Chichester, U.K., 2011.
- (6) Chu, B.; Zhou, X.; Ren, K.; Neese, B.; Lin, M. R.; Wang, Q.; Bauer, F.; Zhang, Q. M. *Science* **2006**, 313, 334–336.
- (7) Kao, K.-C., *Dielectric Phenomena in Solids: with Emphasis on Physical Concepts of Electronic Processes*. Elsevier Academic Press: Boston, MA, 2004.

- (8) Kim, P.; Jones, S. C.; Hotchkiss, P. J.; Haddock, J. N.; Kippelen, B.; Marder, S. R.; Perry, J. W. *Adv. Mater.* **2007**, *19*, 1001–1005.
- (9) Kim, P.; Doss, N. M.; Tillotson, J. P.; Hotchkiss, P. J.; Pan, M. J.; Marder, S. R.; Li, J.; Calame, J. P.; Perry, J. W. *ACS Nano* **2009**, *3*, 2581–2592.
- (10) Li, J.; Claude, J.; Norena-Franco, L. E.; Seok, S. I.; Wang, Q. *Chem. Mater.* **2008**, *20*, 6304–6306.
- (11) Guo, N.; DiBenedetto, S. A.; Kwon, D. K.; Wang, L.; Russell, M. T.; Lanagan, M. T.; Facchetti, A.; Marks, T. J. *J. Am. Chem. Soc.* **2007**, *129*, 766–767.
- (12) Guo, N.; DiBenedetto, S. A.; Tewari, P.; Lanagan, M. T.; Ratner, M. A.; Marks, T. J. *Chem. Mater.* **2010**, *22*, 1567–1578.
- (13) Tang, H.; Lin, Y.; Andrews, C.; Sodano, H. A. *Nanotechnology* **2011**, *22*, 015702.
- (14) Maliakal, A.; Katz, H.; Cotts, P. M.; Subramoney, S.; Mirau, P. J. *Am. Chem. Soc.* **2005**, *127*, 14655–14662.
- (15) Li, J.; Seok, S. I.; Chu, B.; Dogan, F.; Zhang, Q.; Wang, Q. *Adv. Mater.* **2009**, *21*, 217–221.
- (16) Kita, H.; Okamoto, K.; Sakamoto, I. *Radiat. Phys. Chem.* **1986**, *28*, 393–397.
- (17) Zhou, X.; Chu, B.; Neese, B.; Lin, M.; Zhang, Q. M. *IEEE Trans. Dielectr. Electr. Insul.* **2007**, *14*, 1133–1138.
- (18) Lu, Y.; Claude, J.; Neese, B.; Zhang, Q.; Wang, Q. *J. Am. Chem. Soc.* **2006**, *128*, 8120–8121.
- (19) Guan, F.; Wang, J.; Yang, L.; Tseng, J. K.; Han, K.; Wang, Q.; Zhu, L. *Macromolecules* **2011**, *44*, 2190–2199.
- (20) Guan, F.; Wang, J.; Yang, L.; Guan, B.; Han, K.; Wang, Q.; Zhu, L. *Adv. Funct. Mater.* **2011**, *21*, 3176–3188.
- (21) Ma, M.; Vijayan, K.; Hiltner, A.; Baer, E.; Im, J. *J. Mater. Sci.* **1990**, *25*, 2039–2046.
- (22) Kazmierczak, T.; Song, H. M.; Hiltner, A.; Baer, E. *Macromol. Rapid Commun.* **2007**, *28*, 2210–2216.
- (23) Jin, Y.; Tai, H.; Hiltner, A.; Baer, E.; Shirk, J. S. *J. Appl. Polym. Sci.* **2007**, *103*, 1834–1841.
- (24) Weber, M. F.; Stover, C. A.; Gilbert, L. R.; Nevitt, T. J.; Onderkirk, A. *J. Science* **2000**, *287*, 2451–2456.
- (25) Wang, H.; Keum, J. K.; Hiltner, A.; Baer, E.; Freeman, B.; Rozanski, A.; Galeski, A. *Science* **2009**, *323*, 757–760.
- (26) Wolak, M. A.; Pan, M. J.; Wan, A.; Shirk, J. S.; Mackey, M.; Hiltner, A.; Baer, E.; Flandin, L. *Appl. Phys. Lett.* **2008**, *92*, 113301.
- (27) Mackey, M.; Hiltner, A.; Baer, E.; Flandin, L.; Wolak, M. A.; Shirk, J. S. *J. Phys. D: Appl. Phys.* **2009**, *42*, 175304.
- (28) Sawada, A.; Tarumi, K.; Naemura, S. *Jpn. J. Appl. Phys.* **1999**, *38*, 1418–1422.
- (29) Mackey, M.; Schuele, D. E.; Zhu, L.; Baer, E. 2012, to be submitted.
- (30) Ho, J.; Ramprasad, R.; Boggs, S. *IEEE Trans. Dielectr. Electr. Insul.* **2007**, *14*, 1295–1301.
- (31) Buchtemann, A.; Schulz, E. *Thin Solid Films* **1987**, *152*, L135–L138.
- (32) Buchtemann, A.; Geiss, D. *Polymer* **1991**, *32*, 215–220.
- (33) Buchtemann, A.; Schmolke, R. *J. Polym. Sci., Part B: Polym. Phys.* **1991**, *29*, 1299–1302.
- (34) Nalwa, H. S., *Ferroelectric Polymers: Chemistry, Physics, and Applications*; Marcel Dekker, Inc.: New York, 1995.
- (35) Mackey, M.; Flandin, L.; Hiltner, A.; Baer, E. *J. Polym. Sci., Part B: Polym. Phys.* **2011**, *49*, 1750–1761.
- (36) Guan, F.; Pan, J.; Wang, J.; Wang, Q.; Zhu, L. *Macromolecules* **2010**, *43*, 384–392.
- (37) Guan, F.; Wang, J.; Pan, J.; Wang, Q.; Zhu, L. *Macromolecules* **2010**, *43*, 6739–6748.
- (38) Vijayakumar, R. P.; Khakhar, D. V.; Misra, A. *J. Appl. Polym. Sci.* **2010**, *117*, 3491–3497.
- (39) Lovinger, A. *J. Science* **1983**, *220*, 1115–1121.
- (40) Kuffel, E.; Zaengl, W. S.; Kuffel, J., *High Voltage Engineering: Fundamentals*, 2nd ed.; Butterworth-Heinemann: Oxford, U.K., and Boston, MA, 2000.
- (41) Dawber, M.; Chandra, P.; Littlewood, P. B.; Scott, J. F. *J. Phys. Condens. Matter* **2003**, *15*, L393–L398.
- (42) Blinov, L. M.; Fridkin, V. M.; Palto, S. P.; Bune, A. V.; Dowben, P. A.; Ducharme, S. *Usp. Fiz. Nauk* **2000**, *170*, 247–262.
- (43) Rashmi; Narula, G. K.; Pillai, P. K. C. *J. Mater. Sci.* **1987**, *22*, 2006–2010.
- (44) Fanggao, C.; Saunders, G. A.; Lambson, E. F.; Hampton, R. N.; Carini, G.; DiMarco, G.; Lanza, M. *J. Polym. Sci., Part B: Polym. Phys.* **1996**, *34*, 425–433.
- (45) Furukawa, T.; Wang, T. Measurements and Properties of Ferroelectric Polymers. In *The Applications of Ferroelectric Polymers*; Wang, T., Herbert, J. M., Glass, A. M., Eds.; Chapman and Hall: New York, 1988; Vol. 5, pp 66–117.
- (46) Haase, W.; Wróbel, S. *Relaxation Phenomena: Liquid Crystals, Magnetic Systems, Polymers, High-Tc Superconductors, Metallic Glasses*; Springer: New York, 2003.
- (47) Tunçer, E.; Wegener, M.; Gerhard-Multhaup, R. *J. Non-Cryst. Solids* **2005**, *351*, 2917–2921.
- (48) Yano, S.; Okubo, N.; Takahashi, K. *Macromol. Symp.* **1996**, *108*, 279–289.
- (49) Liu, R. Y. F.; Bernal-Lara, T. E.; Hiltner, A.; Baer, E. *Macromolecules* **2005**, *38*, 4819–4827.
- (50) Liu, R. Y. F.; Jin, Y.; Hiltner, A.; Baer, E. *Macromol. Rapid Commun.* **2003**, *24*, 943–948.
- (51) Pierret, R. F., *Semiconductor Device Fundamentals*. Addison-Wesley: Reading, MA, 1996.
- (52) Miyamoto, T.; Shibayam, K. *J. Appl. Phys.* **1973**, *44*, 5372–5376.